The transport properties of graphene

2009 J. Phys.: Condens. Matter 21 323201

(http://iopscience.iop.org/0953-8984/21/32/323201)

IOP PUBLISHING JOURNAL OF PHYSICS: CONDENSED MATTER

J. Phys.: Condens. Matter **21** (2009) 323201 (10pp) doi:10.1088/0953-8984/21/32/323201

TOPICAL REVIEW

The transport properties of graphene

N M R Peres

Department of Physics and Center of Physics, University of Minho, Campus of Gualtar, PT-4710-057, Braga, Portugal

E-mail: peres@fisica.uminho.pt

Received 19 March 2009, in final form 19 May 2009
Published 14 July 2009
Online at stacks.iop.org/JPhysCM/21/323201

Abstract

We review the transport properties of graphene, considering both the case of bulk graphene and that of nanoribbons of this material at zero magnetic field. We discuss: Klein tunneling, transport by evanescent waves when the chemical potential crosses the Dirac point, the conductance of narrow graphene ribbons, the optical conductivity of pristine graphene, and the effect of disorder on the DC conductivity of graphene.

(Some figures in this article are in colour only in the electronic version)

Contents

1. Introduction

Graphene [1, 2] consists of a monolayer of carbon atoms forming a two-dimensional honeycomb lattice. Since this material is a sheet of carbon atoms one atom thick it can be seen as the ultimate thin film ever produced. This material was isolated in 2004 at the University of Manchester, UK, by the group of A K Geim. It has been intensively studied due to its fascinating physical properties [3] and potential applications. There are a number of qualitative reviews on graphene physics in the literature, which will be helpful for the general reader [4–7].

In a certain way, this material was the missing allotrope of pure carbon materials, after the discovery of diamond, graphite, fullerenes, and carbon nanotubes. Although the Manchester team produced other two-dimensional systems [2], graphene attracted wide attention from the community due to its unexpected properties, associated with both fundamental and applied research.

How was graphene first isolated? The original method of graphene production is based on micromechanical cleavage of the graphite surface—the so called Scotch tape method. In very simple terms, a piece of graphite—the material from which pencils are made—is gently rubbed on a piece of ordinary Scotch tape. This produces carbon debris. The Scotch tape with the debris is then pressed against a slab of oxidized silicon (of 300 nm width). As a consequence the debris adhere to the oxidized silicon wafer. Using an optical microscope one can identify small crystallites of graphene on top of the oxidized silicon. This 'low tech' procedure induced a revolution in condensed matter physics.

A carbon atom has six electrons distributed in the atomic orbitals as $1s^2\ 2s^2\ 2p^2$. The 1s electrons are essentially inert and do not contribute to the chemical bond. In graphene, the 2s, $2p_x$ and $2p_y$ orbitals combine—or 'hybridize'—to form three new planar orbitals called sp^2, each containing one electron. The sp^2 orbitals of different atoms then hybridize leading to the formation of the σ bonds. These chemical bonds form an angle of 120° between them and are responsible for the hexagonal lattice structure of graphene. The chemical bonding of the carbon atoms in graphene is maintained by these three orbitals, and the mechanical properties of graphene are determined by the rigidity of the bond. The reader certainly notices that one

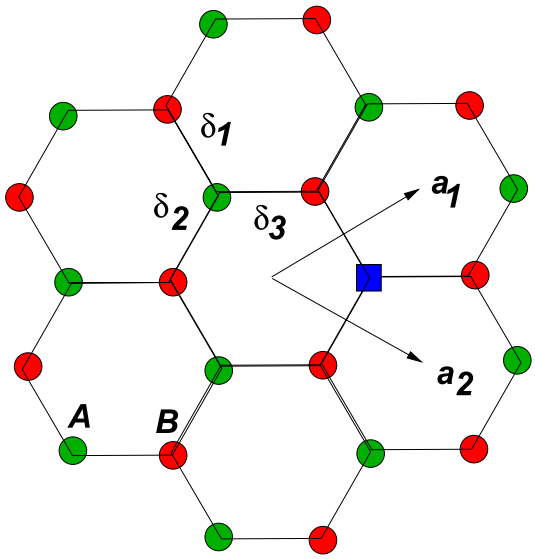

Figure 1. Honeycomb lattice of graphene, with a substituting impurity at the A sublattice (the square). The unit cell vectors $\boldsymbol{a}_1$ and $\boldsymbol{a}_2$ as well as the next nearest neighbor vectors $\boldsymbol{\delta}_i$ ($i = 1, 2, 3$) are also represented.

orbital remains, the p_z orbital with one electron. This orbital is perpendicular to the plane formed by the carbon atoms. As in the case of the sp^2 orbitals, the p_z orbitals of different atoms hybridize to form the π bonds. Each p_z orbital contributes one electron, and therefore graphene is a system with one electron per lattice site (the carbon atoms define the sites in the lattice). This is called a half-filled system. The π orbitals are responsible for the unusual electronic properties of graphene.

As already mentioned, graphene is a two-dimensional hexagonal lattice made of carbon atoms. The hexagonal lattice is not a Bravais lattice. Instead it can be viewed as two interpenetrating triangular lattices, each containing one set of equivalent carbon atom sites—the A and B carbon sites (see figure 1). One should note that from a chemical point of view the two carbon atoms are exactly identical. Since the unit cell contains two carbon atoms, one A and one B, the energy spectrum originating from the π orbitals has two energy bands—a valence band (at lower energies) and a conduction band (at higher energies). As said before, graphene is a half-filled system and therefore the valence band is completely filled. In condensed matter physics, the electronic properties of a system are determined by the nature of the spectrum close to the last filled states, the energy of which defines the Fermi level. Therefore, the physics of graphene is determined by the nature of the energy spectrum close to the top of the valence band and to the bottom of the conduction band. The interaction of the π electrons with the hexagonal lattice gives graphene a very unusual energy spectrum. The nature of the energy spectrum will be clarified in due course.

Graphene's electronic density can be tuned by an external gate voltage (back gate) [1], from electrons to hole charge carriers; the material is very stiff [8], with high thermal conductivity [9], chemically stable and almost impermeable to gases [10], can withstand large current densities [1], and has ballistic transport over submicron scales [1, 11, 12]. These properties alone, and its special geometry, make it a very interesting candidate for applications in nanoelectronics. Recent research has revealed many other possible applications, such as in solar cell technology [13], in liquid crystal devices [14], in single-molecule sensors [15], and in the fabrication of nanosized prototype transistors [16]. Also in fundamental research this material is opening new opportunities to test exciting physical effects [17, 18].

The second exciting result obtained for graphene, after the field effect discovered by the Manchester group [1], was the odd-integer quantum Hall effect [19, 20], also termed the chiral quantum Hall effect. This spectacular effect was predicted by two theoretical groups [21, 22], working independently. As these two groups have shown, this new quantum Hall effect is a consequence of the special nature of the electronic excitations of graphene around the Fermi surface. Equally spectacular is the fact that the quantum Hall effect in graphene can be observed also at room temperatures [23].

If undoped (this is, with zero value of the back gate potential), graphene has one conduction electron per carbon atom. The lattice geometry and its corresponding symmetry group determine the form of the electronic energy as a function of the Bloch momentum. For the electronic density of the undoped system, the Fermi surface is reduced to two independent points in the Brillouin zone and these are labeled $\boldsymbol{K}$ and $\boldsymbol{K}'$. These points are also named Dirac points, for reasons that will become clear in what follows.

As regards the transport properties, one is particularly promising. We refer here to its transparency to light, which is essentially of 97.7%, from the infrared to the ultraviolet. This makes graphene suitable for solar cell industry use, as a transparent electrode. The prototype solar cell produced in [13] explores the fact that only 2.3% of the light shining on graphene is absorbed [24, 25]. This means that graphene has an obvious advantage over the more traditional materials, indium tin oxide (ITO) and fluorine tin oxide (FTO), which have very low transmission of light for wavelengths smaller than 1500 nm. Also these traditional materials have a set of additional problems related to degradation and ion migration [13] which are not shared by graphene. It is therefore important to understand in some detail the mechanism of light absorption in graphene.

The important aspect to address here is how the absorption of light (or its transmission) changes with the wavelength of the incoming light. For light from the infrared to the visible range of the spectrum it is known that the optical conductivity is essentially given by [21, 26–28]

$$\sigma(\omega) = \sigma_0 = \frac{\pi}{2}\frac{e^2}{h}, \tag{1}$$

that is, $\sigma(\omega)$ is constant over the infrared region of the spectrum, given by universal constants, independently of any material parameters. This is a very unusual situation for the optical conductivity of a solid, which in general depends on material parameters, such as the effective mass of the charge carriers and their velocity at the Fermi surface. We shall address in the remainder of the paper this and other aspects related to the transport properties of graphene.

2. Basic concepts

Let us first introduce some definitions for later use. The honeycomb lattice has a unit cell represented in figure 1 by the vectors $\boldsymbol{a}_1$ and $\boldsymbol{a}_2$, such that $|\boldsymbol{a}_1| = |\boldsymbol{a}_2| = a$, with $a \simeq 2.461$ Å. In this basis, any lattice vector $\boldsymbol{r}$ is represented as

$$\boldsymbol{r} = n\boldsymbol{a}_1 + m\boldsymbol{a}_2, \tag{2}$$

with n, m integers. In Cartesian coordinates one has

$$\boldsymbol{a}_1 = \frac{a_0}{2}(3, \sqrt{3}, 0), \qquad \boldsymbol{a}_2 = \frac{a_0}{2}(3, -\sqrt{3}, 0), \tag{3}$$

where $a_0 = a/\sqrt{3}$ is the carbon–carbon distance.

If periodic boundary conditions are used, the Bloch states are characterized by momentum vectors of the form

$$\boldsymbol{k} = \frac{m_1}{N_1}\boldsymbol{b}_1 + \frac{m_2}{N_2}\boldsymbol{b}_2, \tag{4}$$

with m_1 and m_2 a set of integers running from 0 to $N_1 - 1$ and from 0 to $N_2 - 1$, respectively. The numbers N_1 and N_2 are the number of unit cells along the $\boldsymbol{a}_1$ and $\boldsymbol{a}_2$ directions, respectively. The total number of unit cells is, therefore, $N_c = N_1 N_2$. The reciprocal lattice vectors are given by

$$\boldsymbol{b}_1 = \frac{2\pi}{3a_0}(1, \sqrt{3}, 0), \qquad \boldsymbol{b}_2 = \frac{2\pi}{3a_0}(1, -\sqrt{3}, 0). \tag{5}$$

The vectors connecting any A atom to its nearest neighbors read

$$\delta_1 = \frac{a_0}{2}(-1, \sqrt{3}, 0) = \frac{1}{3}(\boldsymbol{a}_1 - 2\boldsymbol{a}_2), \tag{6}$$

$$\delta_2 = \frac{a_0}{2}(-1, -\sqrt{3}, 0) = \frac{1}{3}(\boldsymbol{a}_2 - 2\boldsymbol{a}_1), \tag{7}$$

$$\delta_3 = a_0(1, 0, 0) = \tfrac{1}{3}(\boldsymbol{a}_1 + \boldsymbol{a}_2). \tag{8}$$

The Hamiltonian for pristine graphene can be written as

$$H_0 = -t\sum_{r}[b^\dagger(\boldsymbol{r})a(\boldsymbol{r}) + b^\dagger(\boldsymbol{r} - \boldsymbol{a}_2)a(\boldsymbol{r}) + b^\dagger(\boldsymbol{r} - \boldsymbol{a}_1)a(\boldsymbol{r}) + \text{h.c.}], \tag{9}$$

where $a^\dagger$ ($b^\dagger$) are creation operators for the A (B) sites (the spin index is omitted for simplicity). In the absence of impurities the transport is ballistic. On the other hand, impurities will induce a finite conductivity. The simplest way of modeling the effect of impurities in graphene is by adding an on-site energy which is randomly distributed over the lattice points. The potential at a single site has the form

$$V_i = Ua^\dagger(0)a(0), \tag{10}$$

and its effect on the conductivity of bulk graphene will be studied later. In the particular case $U \to \infty$, the scattering term V_i represents a vacancy. It is well known [29] that the formation of a vacancy will lead to some local distortion of the carbon–carbon bonds. This effect is not incorporated in our Hamiltonian.

For the pristine case the energy bands derived from this Hamiltonian have the form [30]

$$E_\pm(\mathbf{k}) = \pm t\sqrt{3 + f(\mathbf{k})}, \tag{11}$$

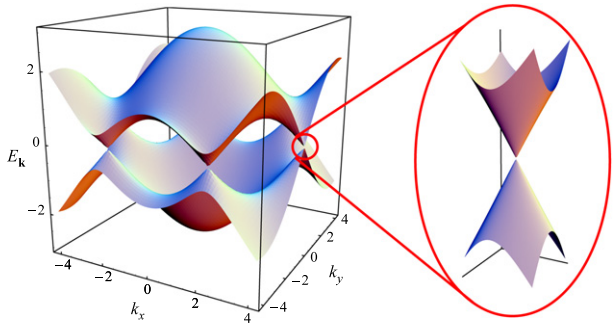

Figure 2. Energy spectrum (in units of t) with a zoom-in of the energy bands close to one of the Dirac points.

with

$$f(\mathbf{k}) = 2\cos(\sqrt{3}k_y a) + 4\cos\left(\frac{\sqrt{3}}{2}k_y a\right)\cos\left(\frac{3}{2}k_x a\right), \tag{12}$$

where the plus sign applies to the upper (π) and the minus sign the lower (π^*) band. Both the valence and the conduction bands are represented in figure 2. A number of interesting and peculiar features emerge from this figure. First it is clear that the valence and the conduction bands touch each other at a number of finite momentum values. The momentum values at which the two bands touch are termed Dirac points (there are two in the Brillouin zone) and are represented by the momentum vectors $\boldsymbol{K}$ and $\boldsymbol{K}'$. As a consequence, graphene's spectrum does not have an energy gap. On the other hand, since the bands only touch at two momentum points the density of states is zero at the corresponding energy. Therefore, graphene is sometimes termed a zero-gap semiconductor with vanishing density of states at the Fermi energy.

In figure 2 we also show a zoom-in of the band structure close to one of the Dirac points. This dispersion can be obtained by expanding the full band structure, equation (11), close to the $\boldsymbol{K}$ (or $\boldsymbol{K}'$) vector as $\boldsymbol{k} = \boldsymbol{K} + \boldsymbol{q}$, with $|\boldsymbol{q}| \ll |\boldsymbol{K}|$ [30]:

$$E_\pm(\boldsymbol{q}) \approx \pm v_F|\boldsymbol{q}| + \mathcal{O}((q/K)^2), \tag{13}$$

where $\boldsymbol{q}$ is the momentum measured relatively to the Dirac points and v_F represents the Fermi velocity, given by $v_F = 3ta/(2\hbar)$, with a value $v_F \simeq 1\times10^6$ m s^{-1}. This result was first obtained by Wallace [30]. We can therefore see graphene bands as the ultrarelativistic limit of the famous Einstein equation $E = \sqrt{m^2c^4 + p^2c^2}$, with $m = 0$ and $c = v_F$, that is, the low energy excitations of graphene are described by massless particles.

Since close to the Dirac point the dispersion is approximated by equation (13) the expression for the density of states per unit cell is given by (with a degeneracy of 4 included, 2 for spin and 2 for the two Dirac points)

$$\rho(E) = \frac{2A_c}{\pi}\frac{|E|}{v_F^2} \tag{14}$$

where A_c is the unit cell area. Additionally, we can show [3] that close to the $\boldsymbol{K}$ point, graphene electrons obey the 2D Dirac

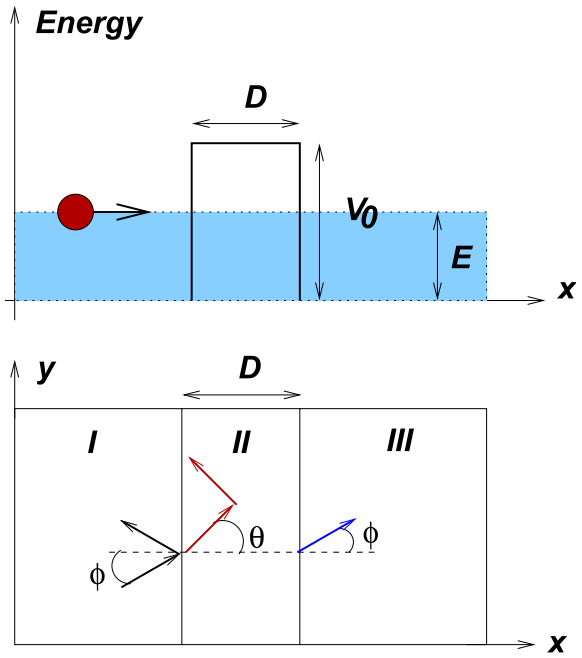

Figure 3. Top: schematic picture of the scattering of Dirac electrons by a square potential. Bottom: definition of the angles ϕ and θ used in the scattering formalism in the three regions I, II, and III.

equation:

$$-\mathrm{i}v_{\mathrm{F}}\boldsymbol{\sigma}\cdot\nabla\psi(\boldsymbol{r}) = E\psi(\boldsymbol{r}), \tag{15}$$

whose wavefunctions have the form $\psi(\boldsymbol{r}) = \psi_{\pm,\boldsymbol{K}}(\boldsymbol{k})\mathrm{e}^{\mathrm{i}\boldsymbol{k}\cdot\boldsymbol{r}}$, with

$$\psi_{\pm,\boldsymbol{K}}(\boldsymbol{k}) = \frac{1}{\sqrt{2}}\begin{pmatrix}\mathrm{e}^{-\mathrm{i}\theta_k/2}\\ \pm\mathrm{e}^{\mathrm{i}\theta_k/2}\end{pmatrix}. \tag{16}$$

3. Klein tunneling

In this section we want to address the scattering of chiral electrons in two dimensions by a square barrier [31, 32]. The one-dimensional scattering of chiral electrons was discussed earlier in the context of carbon nanotubes [33, 34].

We start by noticing that by a gauge transformation the wavefunction (16) can be written as

$$\psi_{\boldsymbol{K}}(\boldsymbol{k}) = \frac{1}{\sqrt{2}}\begin{pmatrix}1\\ \pm\mathrm{e}^{\mathrm{i}\theta_k}\end{pmatrix}. \tag{17}$$

We further assume that the scattering does not mix the momenta around the $\boldsymbol{K}$ and $\boldsymbol{K}'$ points. In figure 3 we depict the scattering process due to the square barrier of width D.

The wavefunction in the different regions can be written in terms of incident and reflected waves. In region I we have

$$\psi_{\mathrm{I}}(\boldsymbol{r}) = \frac{1}{\sqrt{2}}\begin{pmatrix}1\\ s\mathrm{e}^{\mathrm{i}\phi}\end{pmatrix}\mathrm{e}^{\mathrm{i}(k_x x+k_y y)} + \frac{r}{\sqrt{2}}\begin{pmatrix}1\\ s\mathrm{e}^{\mathrm{i}(\pi-\phi)}\end{pmatrix}\mathrm{e}^{\mathrm{i}(-k_x x+k_y y)}, \tag{18}$$

with $\phi = \arctan(k_y/k_x)$, $k_x = k_{\mathrm{F}}\cos\phi$, $k_y = k_{\mathrm{F}}\sin\phi$ and k_{F} the Fermi momentum. In region II we have

$$\psi_{\mathrm{II}}(\boldsymbol{r}) = \frac{a}{\sqrt{2}}\begin{pmatrix}1\\ s'\mathrm{e}^{\mathrm{i}\theta}\end{pmatrix}\mathrm{e}^{\mathrm{i}(q_x x+k_y y)} + \frac{b}{\sqrt{2}}\begin{pmatrix}1\\ s'\mathrm{e}^{\mathrm{i}(\pi-\theta)}\end{pmatrix}\mathrm{e}^{\mathrm{i}(-q_x x+k_y y)}, \tag{19}$$

with $\theta = \arctan(k_y/q_x)$ and

$$q_x = \sqrt{(V_0-E)^2/(v_{\mathrm{F}}^2) - k_y^2}, \tag{20}$$

and finally in region III we have a transmitted wave only:

$$\psi_{\mathrm{III}}(\boldsymbol{r}) = \frac{t}{\sqrt{2}}\begin{pmatrix}1\\ s\mathrm{e}^{\mathrm{i}\phi}\end{pmatrix}\mathrm{e}^{\mathrm{i}(k_x x+k_y y)}, \tag{21}$$

with $s = \mathrm{sgn}(E)$ and $s' = \mathrm{sgn}(E-V_0)$. The coefficients r, a, b and t are determined from the continuity of the wavefunction, which implies that the wavefunction has to obey the conditions $\psi_{\mathrm{I}}(x=0,y) = \psi_{\mathrm{II}}(x=0,y)$ and $\psi_{\mathrm{II}}(x=D,y) = \psi_{\mathrm{III}}(x=D,y)$. Unlike for the Schödinger equation we only need to match the wavefunction and not its derivative. The transmission through the barrier is obtained from $T(\phi) = tt^*$ and has the form

$$T(\phi) = \frac{\cos^2\theta\cos^2\phi}{[\cos(Dq_x)\cos\phi\cos\theta]^2 + \sin^2(Dq_x)(1-ss'\sin\phi\sin\theta)^2}. \tag{22}$$

This expression does not take into account a contribution from evanescent waves in region II, which is usually negligible, unless the chemical potential in region II is at the Dirac energy.

Notice that $T(\phi) = T(-\phi)$ and for values of Dq_x satisfying the relation $Dq_x = n\pi$, with n an integer, the barrier becomes completely transparent since $T(\phi) = 1$, independently of the value of ϕ. Also, for normal incidence ($\phi \to 0$ and $\theta \to 0$) and for any value of Dq_x one obtains $T(0) = 1$, and the barrier is again totally transparent. This result is a manifestation of the Klein paradox [35] and does not occur for non-relativistic electrons. In this latter case and for normal incidence, the transmission is always smaller than 1. In the limit $|V_0| \gg |E|$, equation (22) has the following asymptotic form:

$$T(\phi) \simeq \frac{\cos^2\phi}{1-\cos^2(Dq_x)\sin^2\phi}. \tag{23}$$

In figure 4 we show the angular dependence of $T(\phi)$ for two different values of the potential V_0; it is clear that there are several directions for which the transmission is 1. Similar calculations were done for a graphene bilayer [31] with its most distinctive behavior being the absence of tunneling in the forward ($k_y = 0$) direction. A review of Klein tunneling is available [36] and its consequences have been observed experimentally [37].

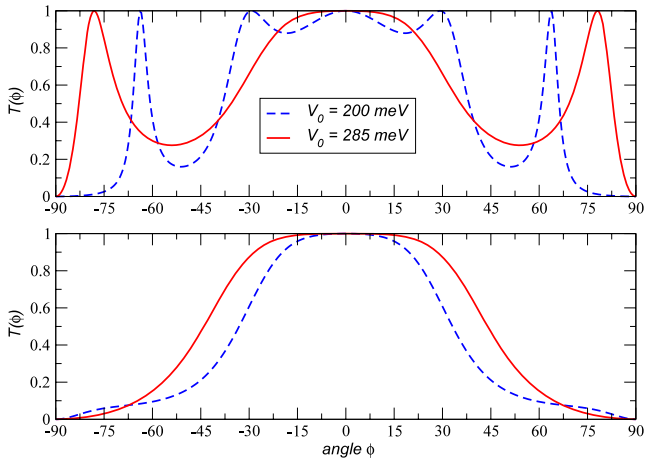

Figure 4. Angular behavior of $T(\phi)$ for two different values of V_0: $V_0 = 200$ meV, dashed line; $V_0 = 285$ meV, solid line. The remaining parameters are $D = 110$ nm (top), $D = 50$ nm (bottom) $E = 80$ meV, $k_F = 2\pi/\lambda$, $\lambda = 50$ nm.

4. The effect of evanescent waves in the transport at the Dirac point

One of the most striking experimental transport results for graphene is its minimum conductivity at the Dirac point. When the chemical potential crosses the Dirac point, the density of charge carriers is zero and therefore it should have zero conductivity. This naive expectation is not what is measured experimentally. In some experiments [41] the data shows that the conductivity at the Dirac point has a finite value—the conductivity minimum—of the order of

$$\sigma_{\min} = \frac{4e^2}{\pi h}. \tag{24}$$

There are two ways of obtaining this result. One is based on the hypotheses that there is a finite concentration, albeit small, of unitary scatterers in graphene [38, 39]. See also [40] for an extended review. The other assumes that the transport is due to evanescent waves in pristine graphene [41–43]. The experiments support this latter view [44].

Let us consider the case of a finite graphene ribbon of width L and length D, as represented in figure 5. The wavefunctions of the free Dirac equation are given by equation (17). The finiteness of the ribbon in the transverse direction imposes that we have to combine two waves of momenta k_y and $-k_y$ in order to satisfy the boundary conditions at the edges of the ribbon. The infinite mass boundary conditions [46] give the following quantization rule for the transverse momentum k_y:

$$k_y L = k_n L = \frac{\pi}{2} + n, \qquad n = 0, \pm 1, \pm 2, \ldots. \tag{25}$$

The wavefunction of the confined electrons reads

$$\psi_{k_x,n} = \frac{e^{ik_x x}}{2\sqrt{L}}\left[\begin{pmatrix} 1 \\ s e^{i\theta(k_x,n)} \end{pmatrix} e^{ik_n y} - i(-1)^n \begin{pmatrix} s e^{i\theta(k_x,n)} \\ 1 \end{pmatrix} e^{-ik_n y}\right], \tag{26}$$

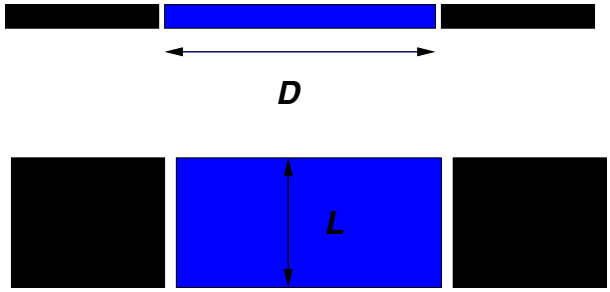

Figure 5. Scheme of a graphene ribbon with width L and length D coupled to two leads also made of graphene.

with

$$\theta(k_x, n) = \arctan\frac{k_n}{k_x}, \tag{27}$$

and $s = \mathrm{sgn}(E)$, where E is the electron energy given by

$$E = \pm v_F \hbar \sqrt{k_x^2 + k_n^2}. \tag{28}$$

As in the case of figure 3, we now assume that there is a region of the ribbon, of width D, where a potential V_g is felt by the electrons in that region. Imposing the continuity of the wavefunction at $x = 0$ and D, the transmission amplitude t is given by

$$t = \frac{(z_{II}^2 + 1)(z_I^2 + 1)}{e^{ik_{II}D}(z_{II} - z_I)^2 + e^{-ik_{II}D}(1 + z_{II}z_I)^2}, \tag{29}$$

where z_I is given by

$$z_I = s\frac{k_I + ik_n}{\sqrt{k_I^2 + k_n^2}}, \tag{30}$$

with k_I given by

$$k_I = \sqrt{\frac{(E - eV_0)^2}{v_F^2\hbar^2} - k_n^2}, \tag{31}$$

where V_0 is the potential applied to graphene in the regions $x < 0$ and $x > D$. In the central region we have k_{II} given by

$$k_{II} = \sqrt{\frac{(E - eV_g)^2}{v_F^2\hbar^2} - k_n^2}. \tag{32}$$

We will be interested in studying the transport when the chemical potential crosses the Dirac point; this makes $V_g = 0$. The transport through the central region can only be maintained by evanescent waves. This is explained in figure 6. Since the chemical potential of the leads, located at $x < 0$ and $x > D$, is at zero energy we have to compute k_I and k_{II} at $E = 0$. This gives propagating modes in the leads for k_n values such that $k_n < e^2V_0^2/(v_F^2\hbar^2)$. In the central region, on the other hand, we have $k_{II} = ik_n$, that is the modes are evanescent waves. In this regime the transmission amplitude for each propagating mode in the leads is given by

$$t_n = \frac{k_I^2 + ik_Ik_n}{\cosh(k_nD)k_I^2 - k_n^2\sinh(k_nD) + ik_Ik_ne^{k_nD}}. \tag{33}$$

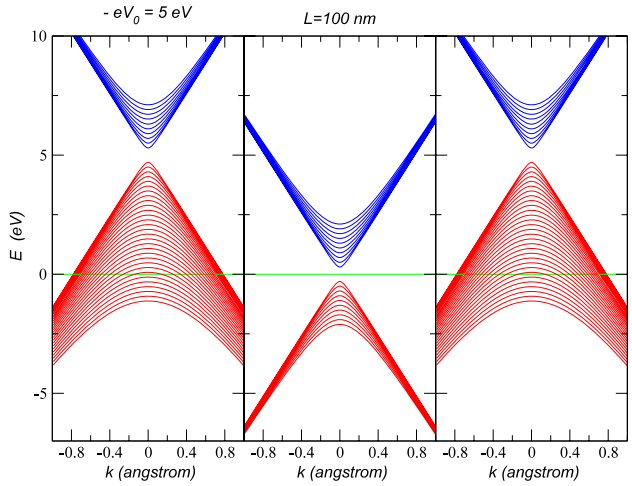

Figure 6. Energy of Dirac electrons in different regions. For $x < 0$ and $x > D$ the energy levels are shifted up in energy and therefore there is a finite density of holes at zero energy. In the central region the potential is zero and the chemical potential crosses the Dirac point.

system is therefore given by

$$G = \frac{4e^2}{h}\sum_{n=0}^{N}|t_n|^2, \tag{34}$$

where N is the maximum number of propagating modes in the leads. The conductivity of the ribbon is then given by

$$\sigma = \frac{D}{L}G. \tag{35}$$

equation (34) can be understood from figure 6, since it makes explicit the transverse modes characterized by k_n; the finiteness of the ribbon produces a number of bands which are all crossed by the chemical potential as long as the condition $k_n < e^2V_0^2/(v_F^2\hbar^2)$ is satisfied. In the case of figure 6 the potential V_0 is negative.

We can see in figure 7 that the conductivity σ tends to the value $\sigma_{\min}$ for large values of the ratio L/D. The conductivity grows away from its minimum value as more electrons are injected into the central region by changing the gate potential V_g.

The curve obtained for G due to evanescent waves should be compared with that obtained using Green's function methods adapted for small ribbons. For comparison we give in figure 8 the transmission $T(E)$ for very narrow ribbons together with the corresponding bands [45]. Both zigzag and armchair ribbons are shown. In the case of armchair ribbons, when the number of rows is a multiple of 3 the system is gapless. The four left panels of figure 8 refer to armchair ribbons, the other panels to zigzag ones. At a given value of the chemical potential μ the conductance G is obtained from $G = 4e^2T(\mu)/h$.

5. Optical conductivity of pristine graphene

It was found by Peres *et al* that the infrared conductivity of graphene is essentially independent of the frequency [39], and

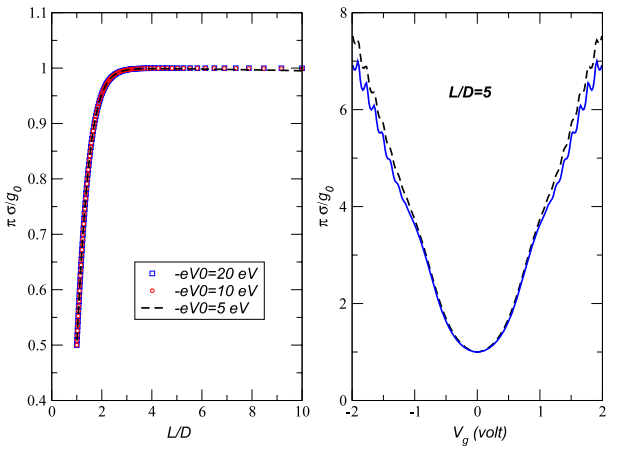

Figure 7. Conductivity of graphene. Left panel: conductivity as a function of the ratio L/D, with L the width of the ribbon and D its length. Right panel: conductivity as a function of gate voltage V_g for a fixed value of L/D. The quantity g_0 equals $4e^2/h$.

given by

$$\sigma(\omega) \simeq \frac{\pi}{2}\frac{e^2}{h}. \tag{36}$$

This result was later reproduced by other groups [47–51]. Later experiments confirmed this result [28, 52].

The calculation of $\sigma(\omega)$ is computed using the Kubo formula. This formula is given by

$$\sigma_{xx}(\omega) = \frac{\langle j_x^D\rangle}{\mathrm{i}A_s(\omega+\mathrm{i}0^+)} + \frac{\Lambda_{xx}(\omega+\mathrm{i}0^+)}{\mathrm{i}\hbar A_s(\omega+\mathrm{i}0^+)}, \tag{37}$$

with $A_s = N_cA_c$ the area of the sample, and $A_c = 3\sqrt{3}a_0^2/2$ (a_0 is the carbon–carbon distance) the area of the unit cell, from which it follows that

$$\mathrm{Re}\,\sigma_{xx}(\omega) = D\delta(\omega) + \frac{\mathrm{Im}\,\Lambda_{xx}(\omega+\mathrm{i}0^+)}{\hbar\omega A_s}, \tag{38}$$

and

$$\mathrm{Im}\,\sigma_{xx}(\omega) = -\frac{\langle j_x^D\rangle}{A_s\omega} - \frac{\mathrm{Re}\,\Lambda_{xx}(\omega+\mathrm{i}0^+)}{\hbar\omega A_s}, \tag{39}$$

where D is the charge stiffness reading

$$D = -\pi\frac{\langle j_x^D\rangle}{A_s} - \pi\frac{\mathrm{Re}\,\Lambda_{xx}(\omega+\mathrm{i}0^+)}{\hbar A_s}. \tag{40}$$

The function $\Lambda_{xx}(\omega+\mathrm{i}0^+)$ is obtained from the Matsubara current–current correlation function, defined as

$$\Lambda_{xx}(\mathrm{i}\omega_n) = \int_0^{\hbar\beta}\mathrm{d}\tau\,\mathrm{e}^{\mathrm{i}\omega_n\tau}\langle T_\tau j_x^P(\tau)j_x^P(0)\rangle. \tag{41}$$

For graphene the current operator reads

$$j_x^P = \frac{tie}{\hbar}\sum_{\boldsymbol{R},\sigma}\sum_{\boldsymbol{\delta}=\boldsymbol{\delta}_1-\boldsymbol{\delta}_3}[\delta_x a_\sigma^\dagger(\boldsymbol{R})b_\sigma(\boldsymbol{R}+\boldsymbol{\delta}) - \mathrm{h.c.}], \tag{42}$$

the function $\mathrm{Im}\,\Lambda_{xx}(\omega+\mathrm{i}0^+)$ in the Kubo formula is given by

$$\mathrm{Im}\,\Lambda_{xx}(\omega+\mathrm{i}0^+) = \frac{t^2e^2a^2}{8\hbar^2} \times \sum_{\boldsymbol{k}} f[\phi(\boldsymbol{k})][n_F(-t|\phi(\boldsymbol{k})|-\mu) - n_F(t|\phi(\boldsymbol{k})|-\mu)] \times [\pi\delta(\omega-2t|\phi(\boldsymbol{k})|/\hbar) - \pi\delta(\omega+2t|\phi(\boldsymbol{k})|/\hbar)], \tag{43}$$

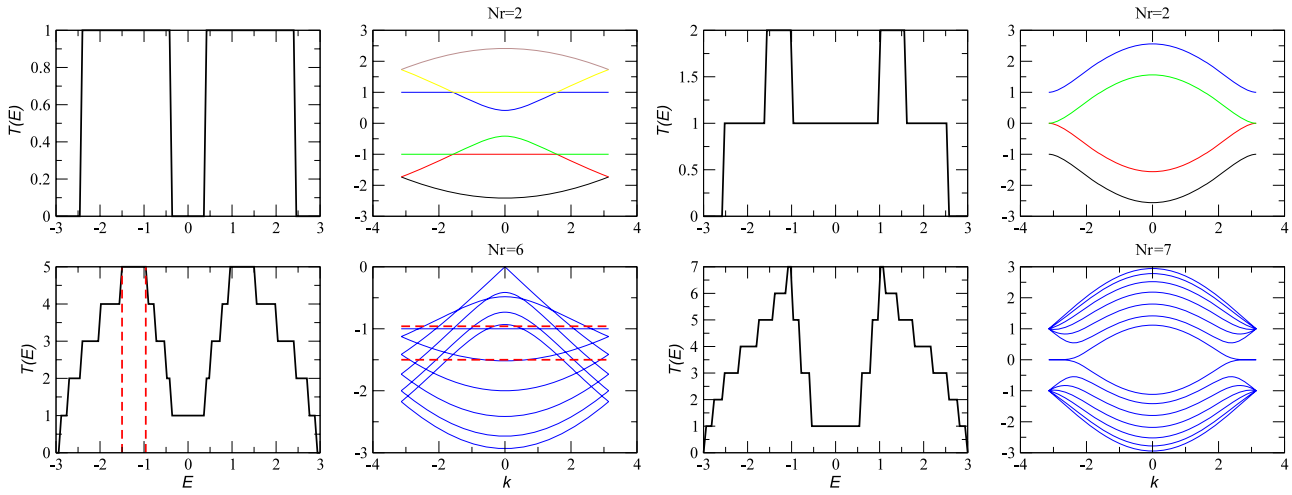

Figure 8. Transmission $T(E)$ and energy bands for different types of graphene ribbons. The conductance is given by $G = 4e^2T(\mu)/h$.

where $n_F(x)$ is the usual Fermi distribution, μ is the chemical potential, and the function $\mathrm{Re}\,\Lambda_{xx}(\omega + \mathrm{i}0^+)$ is given by

$$\mathrm{Re}\,\Lambda_{xx}(\omega + \mathrm{i}0^+) = -\frac{t^2e^2a^2}{8\hbar^2}\mathcal{P} \times \sum_{\boldsymbol{k}} f[\phi(\boldsymbol{k})][n_F(-t|\phi(\boldsymbol{k})| - \mu) - n_F(t|\phi(\boldsymbol{k})| - \mu)] \times \frac{4t|\phi(\boldsymbol{k})|}{\omega^2 - (2|\phi(\boldsymbol{k})|)^2}, \tag{44}$$

with

$$f[\phi(\boldsymbol{k})] = 18 - 4|\phi(\boldsymbol{k})|^2 + 18\frac{[\mathrm{Re}\,\phi(\boldsymbol{k})]^2 - [\mathrm{Im}\,\phi(\boldsymbol{k})]^2}{|\phi(\boldsymbol{k})|^2}, \tag{45}$$

and $\mathcal{P}$ denoting the principal part of the integral. The graphene energy bands are given by $\epsilon(\boldsymbol{k}) = \pm t|\phi(\boldsymbol{k})|$, with $\phi(\boldsymbol{k})$ defined as

$$\phi(\boldsymbol{k}) = 1 + \mathrm{e}^{\boldsymbol{k}\cdot(\boldsymbol{\delta}_1 - \boldsymbol{\delta}_3)} + \mathrm{e}^{\boldsymbol{k}\cdot(\boldsymbol{\delta}_2 - \boldsymbol{\delta}_3)}. \tag{46}$$

Equation (44) is completely general. Since we want to derive an expression for $\sigma(\omega)$ valid up to visible frequencies, we need to extend the density of states away from the Dirac point. Doing this we obtain [53]

$$\rho(E) \simeq \frac{2E}{\sqrt{3}\pi t^2} + \frac{2E^3}{3\sqrt{3}\pi t^4} + \frac{10E^5}{27\sqrt{3}\pi t^6}. \tag{47}$$

Using equation (47) in (44) we obtain for the optical conductivity the approximate result

$$\mathrm{Re}\,\sigma_{xx}(\omega) = \sigma_0\left(\frac{1}{2} + \frac{1}{72}\frac{(\hbar\omega)^2}{t^2}\right) \times \left(\tanh\frac{\hbar\omega + 2\mu}{4k_BT} + \tanh\frac{\hbar\omega - 2\mu}{4k_BT}\right). \tag{48}$$

In the case of $\mu = 0$ this expression is the same as in Kuzmenko *et al* [28] and in Falkovsky *et al* [54–56] if in both cases the $(\hbar\omega/t)^2$ term is neglected.

We can then use the expression obtained for the conductivity to compute the transmission of light through graphene. The calculation uses a Fresnel type of analysis, including the fact that graphene may dissipate a percentage of the incident light. Working this out we obtain [53, 57]

$$T = \frac{1}{(1 + \pi\alpha/2)^2} \simeq 1 - \pi\alpha, \tag{49}$$

where $\alpha = e^2/(4\pi\epsilon_0 c\hbar)$ is the fine structure constant. That graphene and its bilayer are transparent to visible light can be seen in figure 9, which shows a picture of a graphene membrane taken with an optical microscope. The picture shows a graphene membrane covering a hole in a metallic scaffold. We can see that a part of the hole is not covered with graphene and the other part is covered with graphene and bilayer graphene. The transmittance of light changes as we move from air to the bilayer. The experimental values for T are given in figure 10 and they agree well with equation (49).

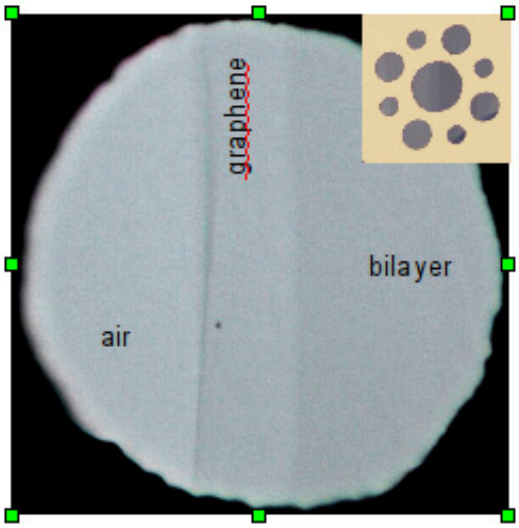

Figure 9. The figure shows a photo of a graphene membrane as seen with an optical microscope. Reproduced with permission of [24]. Copyright 2008, by the AAAS.

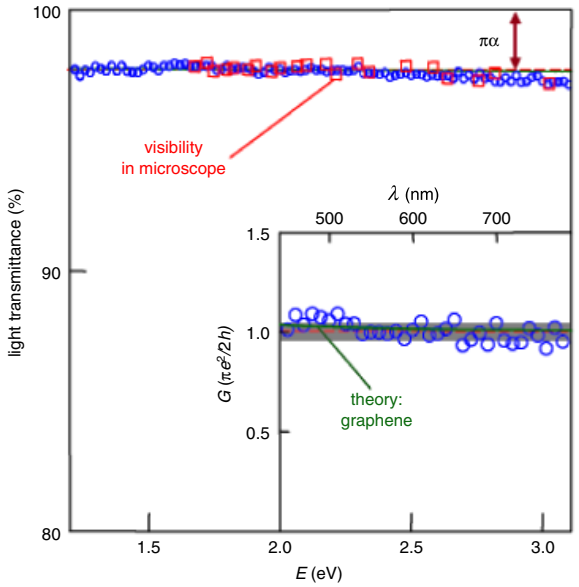

Figure 10. The figure shows the measured transmittance of graphene T, which agrees well with equation (49), as seen in the inset. Reproduced with permission of [24]. Copyright 2008, by the AAAS.

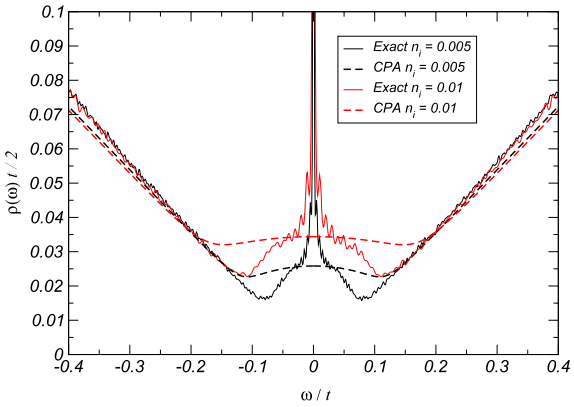

Figure 11. Density of states of graphene in the presence of mid-gap states. The CPA calculation is compared with a numerical exact method. The concentration of impurities is $n_i = 0.005$ and $n_i = 0.01$. Here and in the following figures we use $t = 3$ eV and a cutoff energy of $D = 7$ eV.

6. Conductivity of disordered graphene

We now want to consider the effect of impurities on the DC conductivity of graphene. We will consider two kinds of impurities: unitary scatterers and charged impurities.

6.1. Unitary scatterers

The physical origin of mid-gap states in graphene is varied. Cracks, edges, vacancies [58] are all possible sources for mid-gap states. From an analytical point of view, these kinds of impurities (scatterers) are easily modeled by considering the effect of vacancies. We stress, however, that this route is chosen due to its analytic simplicity.

The effect of mid-gap states on the conductivity of graphene was first considered by Peres *et al* [39] for the case of a half-filled system. Considering the effect of a local scattering potential of intensity U, such as that given by equation (10), the electronic Green's function in the Dirac cone approximation has the form [60, 61]

$$G = \frac{\begin{pmatrix} \mathrm{i}\omega_n - \Sigma(\mathrm{i}\omega_n) & -t\phi(\boldsymbol{k}) \\ -t\phi^*(\boldsymbol{k}) & \mathrm{i}\omega_n - \Sigma(\mathrm{i}\omega_n) \end{pmatrix}}{[\mathrm{i}\omega_n - \Sigma(\mathrm{i}\omega_n)][\mathrm{i}\omega_n - \Sigma(\mathrm{i}\omega_n)] - t^2|\phi(\boldsymbol{k})|^2}, \tag{50}$$

with the retarded self-energy

$$\Sigma^{\mathrm{ret}}_{\mathrm{unit}}(\omega) = \frac{n_i U}{\hbar} \frac{1 - UF(\omega) - \mathrm{i}U\pi R(\omega)}{[1 - UF(\omega)]^2 + [U\pi R(\omega)]^2}, \tag{51}$$

where the functions $F(\omega)$ and $R(\omega)$ are defined by

$$\frac{1}{\hbar N_c} \sum_{\boldsymbol{k}} G(\boldsymbol{k}, \omega + \mathrm{i}0^+) = F(\omega) - \mathrm{i}\pi R(\omega). \tag{52}$$

Mid-gap states are obtained by making the limit $U \to \infty$, which corresponds to the unitary limit. Clearly, $R(\omega)$ is the density of states per spin per unit cell. For latter use, we write the self energy due to unitary scatterers, $\Sigma^{\mathrm{ret}}_{\mathrm{unit}}(\omega)$, as a sum of real and imaginary parts, $\Sigma^{\mathrm{ret}}_{\mathrm{unit}}(\omega) = \Sigma'(\omega) + \mathrm{i}\Sigma''(\omega)$ (note that $\Sigma'' > 0$). The functions $F(\omega)$ and $R(\omega)$ are determined self-consistently through a well defined numerical procedure [60, 61].

In figure 11, we compare the density of states computed using the coherent potential approximation (CPA) equations with that obtained from a numerical exact method [59]. It is clear that the CPA captures the formation of mid-gap states in a quantitative way. The main difference is the presence of a peak at zero energy in the exact density of states, whose measure is quantitatively negligible.

6.2. Charged scatterers

It has been argued that charged impurities are crucial for understanding the transport properties of graphene on top of a silicon oxide substrate [62–64]. In what follows, we compute the electronic self-energy due to charge impurities, using second-order perturbation theory in the scattering potential. Electronic scattering from an impurity of charge eQ_c leads to a term in the Hamiltonian of the form

$$V = -\sum_{r,\sigma} \frac{Q_c e^2}{\sqrt{d^2 + \boldsymbol{r}^2}} [a^\dagger_\sigma(\boldsymbol{r}) a_\sigma(\boldsymbol{r}) + b^\dagger_\sigma(\boldsymbol{r}) b_\sigma(\boldsymbol{r})], \tag{53}$$

where d is the distance from the impurity to the graphene plane. In momentum space, V reads

$$V = \frac{1}{N_c} \sum_{\boldsymbol{p},\boldsymbol{q},\sigma} V_0(\boldsymbol{q}) [a^\dagger_\sigma(\boldsymbol{p}) a_\sigma(\boldsymbol{p}+\boldsymbol{q}) + b^\dagger_\sigma(\boldsymbol{p}) b_\sigma(\boldsymbol{p}+\boldsymbol{q})], \tag{54}$$

where $V_0(\boldsymbol{q})$ reads

$$V_0(\boldsymbol{q}) = -\sum_r \frac{Q_c e^2 \mathrm{e}^{\mathrm{i}\boldsymbol{r}\cdot\boldsymbol{q}}}{\sqrt{d^2 + \boldsymbol{r}^2}}. \tag{55}$$

With $G^0(\boldsymbol{k}, \mathrm{i}\omega_n)$ the bare and $G(\boldsymbol{k}, \boldsymbol{p}, \mathrm{i}\omega_n)$ the full Green's functions, the Dyson equation due to one Coulomb impurity

reads

$$G(\boldsymbol{k},\boldsymbol{p},\omega_n) = \delta_{k,p}G^0(\boldsymbol{k},\mathrm{i}\omega_n) + G^0(\boldsymbol{k},\mathrm{i}\omega_n)\frac{1}{\hbar N_\mathrm{c}}\sum_{k'} V_0(\boldsymbol{k}-\boldsymbol{k}')G(\boldsymbol{k}',\boldsymbol{p},\omega_n). \quad (56)$$

If we consider a finite density of charged impurities per unit cell, n_i^C, and incoherent scattering between impurities, the second-order self-energy is given by

$$\Sigma^{\mathrm{ret}}_{\mathrm{Coul}}(\boldsymbol{k},\mathrm{i}\omega_n) = \frac{n_i^C}{\hbar^2 N_\mathrm{c}}\sum_{p} V^2(\boldsymbol{k}-\boldsymbol{p})G^0(\boldsymbol{p},\mathrm{i}\omega_n), \quad (57)$$

where a term proportional to $V(0)$ was absorbed in the chemical potential, since it corresponds to an energy shift only. Note that we have replaced $V_0(\boldsymbol{q})$ by $V(\boldsymbol{q})$, which corresponds to including the effect of electronic screening in the calculation. The form of $V(\boldsymbol{q})$ is (in SI units) [65, 66]

$$V(\boldsymbol{q}) = -\frac{Q_\mathrm{c}e^2}{2\epsilon_0\epsilon A_\mathrm{c}}\frac{\mathrm{e}^{-qd}}{q+\gamma}, \quad (58)$$

where $\epsilon = 3.9$ is the silicon oxide relative permittivity and γ is given by

$$\gamma = \frac{\rho(\mu)e^2}{2\epsilon_0\epsilon A_\mathrm{c}}, \quad (59)$$

where $\rho(\mu)$ is the self-consistent density of states as computed from the CPA calculation ($A_\mathrm{c} = 3\sqrt{3}a_0^2/2$ is the area of the unit cell).

The self-energy (57) is dependent both on the momentum $\boldsymbol{k}$ and on the frequency. However, we are interested in the effect of the self-energy for momentum close to the Dirac point. Within this approximation the imaginary part of the retarded self-energy becomes diagonal and momentum independent, reading ($d \simeq 0$)

$$\hbar\,\mathrm{Im}\,\Sigma^{\mathrm{ret}}_{\mathrm{Coul}}(\boldsymbol{K},\omega) \simeq -n_i^C\frac{Q_\mathrm{c}^2e^4}{4A_\mathrm{c}^2\epsilon_0^2\epsilon}\frac{1}{\sqrt{3}t^2}|\hbar\omega|\left(\frac{2|\hbar\omega|}{3ta}+\gamma\right)^{-2}. \quad (60)$$

Let us now discuss the conductivity as a function of the gate voltage V_g, which relates to the chemical potential as $V_\mathrm{g} \propto \mu^2$. In figure 12 we show σ as a function of V_g considering both charged impurities and short range scatterers. It is well known that when one considers only charged impurities, σ is linear in V_g [62, 63, 65, 66], being zero at the Dirac point. Further, within the first Born approximation the conductivity does not show particle–hole asymmetry. A more rigorous treatment shows that even Coulomb impurities can lead to particle–hole asymmetry [67–69].

On the other hand, considering short range impurities with a finite strength U a clear particle–hole asymmetry develops, with a strong suppression of the conductivity in the hole or particle sector, depending on the sign of U. If the density of short range impurities decreases, the conductivity, albeit mostly controlled by charged impurities, still has fingerprints of the finite U scatterers, due to the asymmetry between the hole and particle branches.

If we suppress the scattering due to charged impurities, which would be the case in suspended graphene, only the scattering due to short range scatterers survive. In this case it should be possible to decide whether the short range impurities are in the unitary regime, in which case the conductivity will symmetric relatively to the Dirac point, or having a finite U value, in which case an asymmetry between the hole and the particle branches of the conductivity curve should be observed. We note that asymmetric conductivity curves were recently observed [70]. Other groups have also reported theoretical results on the particle–hole asymmetry of graphene's conductivity [67–69, 71, 72].

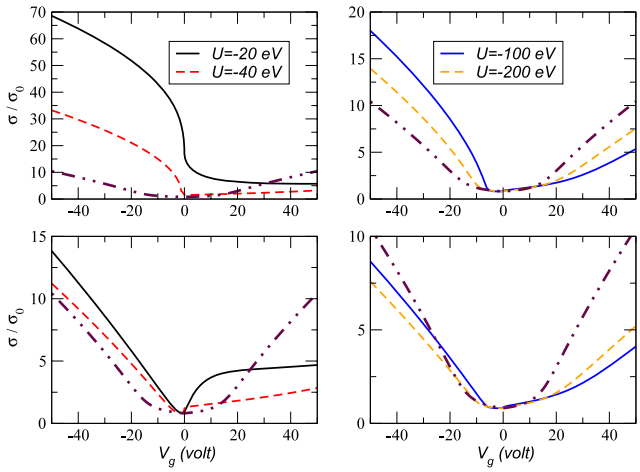

Figure 12. Upper panels: conductivity $\sigma(V_\mathrm{g})$, in units of $\sigma_0 = \pi e^2/(2h)$, for different values of U. Lower panels: conductivity $\sigma(\mu)$ including the effect of charge scatterers. The concentration per unit cell of short range scatterers is $n_i = 10^{-3}$ and that of charged ones is $n_i^C = 10^{-4}$. The dashed–dotted line is the conductivity for unitary scatterers of concentration $n_i = 10^{-3}$ with zero density of charge scatterers.

7. Summary

We have reviewed several aspects of the transport properties of graphene, considering both ribbons and bulk graphene. In the ribbon case, the transport is sensitive to the transverse modes of the system. For bulk graphene, the Dirac spectrum mainly controls the behavior of the transport properties. We have seen that in the case of disordered graphene the existence of scatterers with a finite strength induces an asymmetry between the hole and particle region of the conductivity.

Acknowledgments

NMRP acknowledges financial support from POCI 2010 via project PTDC/FIS/64404/2006 and helpful discussion with Andre Geim, Antonio Castro Neto, Eduardo Castro, Francisco Guinea, João Lopes dos Santos, Tobias Stauber, and Vitor Pereira.

References

[1] Novoselov K S, Geim A K, Morozov S V, Jiang D, Zhang Y, Dubonos S V, Grigorieva I V and Firsov A A 2004 *Science* **306** 666

[2] Novoselov K S, Jiang D, Booth T, Khotkevich V V, Morozov S M and Geim A K 2005 *Proc. Natl Acad. Sci.* **102** 10451

[3] Castro Neto A H, Guinea F, Peres N M R, Novoselov K S and Geim A K 2009 *Rev. Mod. Phys.* **81** 109
[4] Geim A K and Novoselov K S 2007 *Nat. Mater.* **6** 183
[5] Castro Neto A H, Guinea F and Peres N M R 2006 *Phys. World* **19** 33
[6] Geim A K and MacDonald A H 2007 *Phys. Today* **60** 35
[7] Geim A K and Kim P 2008 *Sci. Am.* (April) 90
[8] Booth T J, Blake P, Nair R R, Jiang D, Hill E W, Bangert U, Bleloch A, Gass M, Novoselov K S, Katsnelson M I and Geim A K 2008 arXiv:0805.1884v4 [cond-mat.mes-hall]
[9] Balandin A A, Ghosh S, Bao W, Calizo I, Teweldebrhan D, Miao F and Lau C N 2008 *Nano Lett.* **8** 902
[10] Bunch J S, Verbridge S S, Alden J S, van der Zande A M, Parpia J M, Craighead H G and McEuen P L 2008 arXiv:0805.3309v1 [cond-mat.mtrl-sci]
[11] Morozov S V, Novoselov K S, Katsnelson M I, Schedin F, Elias D C, Jaszczak J A and Geim A K 2008 *Phys. Rev. Lett.* **100** 016602
[12] Bolotin K I, Sikes K J, Jiang Z, Klima M, Fudenberg G, Hone J, Kim P and Stormer H L 2008 *Solid State Commun.* **146** 351
[13] Wangzhi L X and Mullen K 2008 *Nano Lett.* **8** 323
[14] Blake P, Brimicombe P D, Nair R R, Booth T J, Jiang D, Schedin F, Ponomarenko L A, Morozov S V, Gleeson H F, Hill E W, Geim A K and Novoselov K S 2008 *Nano Lett.* **8** 1704
[15] Schedin F, Geim A K, Morozov S V, Jiang D, Hill E H, Blake P and Novoselov K S 2007 *Nat. Mater.* **6** 652
[16] Wang X, Ouyang Y, Li X, Wang H, Guo J and Dai H 2008 *Phys. Rev. Lett.* **100** 206803
[17] Ponomarenko L A, Schedin F, Katsnelson M I, Yang R, Hill E H, Novoselov K S and Geim A K 2008 *Science* **320** 356
[18] Cheianov V V, Fal'ko V and Altshuler B L 2007 *Science* **315** 1252
[19] Novoselov K S, Geim A K, Morozov S V, Jiang D, Katsnelson M I, Grigorieva I V, Dubonos S V and Firsov A A 2005 *Nature* **438** 197
[20] Zhang Y, Tan Y-W, Stormer H L and Kim Philip 2005 *Nature* **438** 201
[21] Peres N M R, Guinea F and Castro Neto A H 2006 *Phys. Rev.* B **73** 125411
[22] Gusynin V P and Sharapov S G 2005 *Phys. Rev. Lett.* **95** 146801
[23] Novoselov K S, Jiang Z, Zhang Y, Morozov S V, Stormer H L, Zeitler U, Maan J C, Boebinger G S, Kim P and Geim A K 2007 *Science* **315** 1379
[24] Nair R R, Blake P, Grigorenko A N, Novoselov K S, Booth T J, Stauber T, Peres N M R and Geim A K 2008 *Science* **320** 1308
[25] Stauber T, Peres N M R and Geim A K 2008 *Phys. Rev.* B **78** 085432
[26] Gusynin V P, Sharapov S G and Carbotte J P 2007 *Int. J. Mod. Phys.* B **21** 4611
[27] Peres N M R and Stauber T 2008 *Int. J. Mod. Phys.* B **22** 2529
[28] Kuzmenko A B, Van Heumen E, Carbone F and van der Marel D 2008 *Phys. Rev. Lett.* **100** 117401
[29] El-Barbary A A, Telling R H, Ewels C P, Heggie M I and Briddon P R 2003 *Phys. Rev.* B **68** 144107
[30] Wallace P R 1947 *Phys. Rev.* **71** 622
[31] Katsnelson M I, Novoselov K S and Geim A K 2006 *Nat. Phys.* **2** 620
[32] Katsnelson M I 2007 *Mater. Today* **10** 20
[33] Ando T, Nakanishi T and Saito R 1998 *J. Phys. Soc. Japan* **67** 2857
[34] McEuen P L, Bockrath M, Cobden D H, Yoon Y-G and Louie S G 1999 *Phys. Rev. Lett.* **83** 5098
[35] Calogeracos A and Dombey N 1999 *Contemp. Phys.* **40** 313
[36] Beenakker C W J 2008 *Rev. Mod. Phys.* **80** 1337
[37] Stander N, Huard B and Goldhaber-Gordon D 2009 *Phys. Rev. Lett.* **102** 026807
[38] Shon N H and Ando T 1998 *J. Phys. Soc. Japan* **67** 2421
[39] Peres N M R, Guinea F and Castro Neto A H 2006 *Phys. Rev.* B **73** 125411
[40] Cresti A, Nemec N, Biel B, Niebler G, Triozon F, Cuniberti G and Roche S 2008 *Nano Res.* **1** 361
[41] Tworzydlo J, Trauzettel B, Titov M, Rycerz A and Beenakker C W J 2006 *Phys. Rev. Lett.* **96** 246802
[42] Katsnelson M I 2006 *Eur. Phys. J.* B **51** 157
[43] Ziegler K 2007 *Phys. Rev.* B **75** 233407
[44] Miao F, Wijeratne S, Zhang Y, Coskun U C, Bao W and Lau C N 2007 *Science* **317** 1530
[45] Wakabayashi K, Fujita M, Ajiki H and Sigrist M 1999 *Phys. Rev.* B **59** 8271
Wakabayashi K and Sigrist M 2000 *Phys. Rev. Lett.* **84** 3390
Wakabayashi K 2001 *Phys. Rev.* B **64** 125428
Wakabayashi K, Takane Y and Sigrist M 2007 *Phys. Rev. Lett.* **99** 036601
[46] Berry M V and Mondragon R J 1987 *Proc. R. Soc.* A **412** 53
[47] Gusynin V P and Sharapov S G 2006 *Phys. Rev.* B **73** 245411
[48] Gusynin V P, Sharapov S G and Carbotte J P 2006 *Phys. Rev. Lett.* **96** 256802
[49] Gusynin V P, Sharapov S G and Carbotte J P 2007 *Phys. Rev. Lett.* **98** 157402
[50] Gusynin V P, Sharapov S G and Carbotte J P 2007 *Phys. Rev.* B **75** 165407
[51] Gusynin V P, Sharapov S G and Carbotte J P 2007 *Int. J. Mod. Phys.* B **21** 4611
[52] Li Z Q, Henriksen E A, Jiang Z, Hao Z, Martin M C, Kim P, Stormer H L and Basov D N 2008 *Nat. Phys.* **4** 532
[53] Stauber T, Peres N M R and Geim A K 2008 *Phys. Rev.* B **78** 085432
[54] Falkovsky L A and Varlamov A A 2007 *Eur. Phys. J.* B **56** 281
[55] Falkovsky L A and Pershoguba S S 2007 *Phys. Rev.* B **76** 153410
[56] Falkovsky L A 2008 *J. Exp. Theor. Phys.* **106** 575
[57] Nair R R, Blake P, Grigorenko A N, Novoselov K S, Booth T J, Stauber T, Peres N M R and Geim A K 2008 *Science* **320** 1308
[58] Eberlein T, Bangert U, Nair R R, Jones R, Gass M, Bleloch A L, Novoselov K S, Geim A and Briddon P R 2008 *Phys. Rev.* B **77** 233406
[59] Vitor Pereira M, Guinea F, Lopes dos Santos J M B, Peres N M R and Castro Neto A H 2006 *Phys. Rev. Lett.* **96** 036801
[60] Stauber T, Peres N M R and Castro Neto A H 2008 *Phys. Rev.* B **78** 085418
[61] Peres N M R, Stauber T and Castro Neto A H 2008 *Europhys. Lett.* **84** 38002
[62] Nomura K and MacDonald A H 2007 *Phys. Rev. Lett.* **98** 076602
[63] Adam S, Hwang E H, Galitski V M and Das Sarma S 2007 *Proc. Natl Acad. Sci. USA* **104** 18392
[64] Chen J H, Jang C, Fuhrer M S, Williams E D and Ishigami M 2008 *Nat. Phys.* **4** 377
[65] Peres N M R, Lopes dos Santos J M B and Stauber T 2007 *Phys. Rev.* B **76** 073412
[66] Stauber T, Peres N M R and Guinea F 2007 *Phys. Rev.* B **76** 205423
[67] Pereira V M, Nilsson J and Castro Neto A H 2007 *Phys. Rev. Lett.* **99** 166802
[68] Shytov A V, Katsnelson M I and Levitov L S 2007 *Phys. Rev. Lett.* **99** 236801
[69] Novikov D S 2007 *Appl. Phys. Lett.* **91** 102102
[70] Du X, Skachko I, Barker A and Andrei E Y 2008 *Nat. Nanotechnol.* **3** 491
[71] Lherbier A, Biel B, Niquet Y-M and Roche S 2008 *Phys. Rev. Lett.* **100** 036803
[72] Robinson J P, Schomerus H, Oroszlny L and Fal'ko V I 2008 *Phys. Rev. Lett.* **101** 196803